JGE (Jurnal Geofisika Eksplorasi)
Vol. 08 No. 02, Juli 2022 (113-126) https://doi.org/ 10.23960/jge.v8i2.204

# APPLICATION OF GENERALIZED DERIVATIVE OPERATOR ON BOUGUER ANOMALY FOR DETECTING GEOLOGICAL STRUCTURES

# *APLIKASI OPERATOR TURUNAN UMUM PADA ANOMALI BOUGUER UNTUK MENDETEKSI STRUKTUR GEOLOGI*

**Dicky Ahmad Zaky[1*], Alissa Bilqis[2]**

[1,2]Geophysical Engineering Department; Universitas Pertamina
[1]Center for Geosciences Artificial Intelligence and Advanced Computing; Universitas Pertamina

Received: 2022, February 21st
Accepted: 2022, May 7th

**Keywords:**
Analytic signal amplitude;
Generalized derivative operator;
Horizontal gradient;
Second Vertical Derivative.

**Corespondent Email:**
dicky.az@universitas pertamina.ac.id

**How to cite this article**:
Zaky, D. A. & Bilqis, A. (2022). Application of Generalized Derivative Operator on Bouguer Anomaly for Detecting Geological Structures. *Jurnal Geofisika Eksplorasi*, 08(02), 113-126.

**Abstract.** Generalized Derivative Operator (GDO) is one of the first-order derivative filters that could control the derivative's direction by modifying the value of azimuth ($\theta$) and dip ($\phi$) parameters. This study aims to examine those GDO parameters on synthetic Bouguer anomaly and apply them to field data of the Silver Peak geothermal field to identify the geological structures. We use Python programs to conduct the GDO and other derivative operators such as horizontal gradient (HG), analytic signal amplitude (AS), as well Second Vertical Derivative (SVD) for comparison. The derivative operators are performed in the Fourier domain and spatial domain. The results from synthetic data show that GDO can amplify the response both on local and regional anomalies. Nevertheless, enhanced local and regional anomaly might be shown as the same maximum value of GDO. It appears that GDO disregard the influence of density contrast and depth variation of the anomalous body. Subsequently, anomaly enhancement of Silver Peak area shows that GDO anomaly concurred with geological map. GDO and SVD could amplify the response of geological structures such as intrusive granite, fault lineaments, and lithological contact, as well as the horst-graben structure, as mentioned in previous studies, that might be acting as fluid pathways for the Silver Peak geothermal system.

**Abstrak.** *Operator Turunan Umum atau Generalized Derivative Operator (GDO) merupakan salah satu filter turunan orde pertama yang mampu mengontrol arah turunan dengan memodifikasi nilai parameter sudut azimut* ($\theta$) *dan kemiringan* ($\phi$). *Penelitian ini bertujuan untuk menguji parameter GDO pada anomali Bouguer sintetik dan mengaplikasikannya pada data di lapangan panasbumi Silver Peak untuk mengidentifikasi struktur geologi. Kami menggunakan program Python untuk menerapkan GDO dan operator turunan lainnya seperti,* horizontal gradient (HG), analytic signal amplitude (AS) *serta* Second Vertical Derivative (SVD) *sebagai pembanding. Operator turunan*

© 2022 JGE (Jurnal Geofisika Eksplorasi). This article is an open-access article distributed under the terms and conditions of the Creative Commons Attribution (CC BY NC)

*dilakukan dalam domain Fourier dan domain spasial. Hasil dari pengujian data sintetik menunjukkan bahwa GDO mampu untuk meningkatkan respon baik dari anomali lokal maupun regional. Namun demikian, anomali lokal dan regional yang ditingkatkan mungkin saja menunjukkan nilai maksimum GDO yang sama, tampaknya GDO mengabaikan pengaruh dari variasi kontras densitas dan kedalaman dari sumber anomali. Selanjutnya, peningkatan anomali di area Silver Peak menunjukkan bahwa anomali GDO sesuai dengan peta geologi. GDO dan SVD dapat meningkatkan respon dari struktur geologi seperti, intrusi granit, kemenerusan sesar, dan kontak litologi, serta struktur horst-graben yang disebutkan dalam studi terdahulu, yang mungkin berperan sebagai jalur fluida sistem panasbumi Silver Peak.*

## 1. INTRODUCTION

Anomaly enhancement and isolation using the derivative of potential field data such as gravity data is generally used in almost all geophysical exploration. Most of them are intended to understand the geological features and structures around the surveyed area which are often covered by regional responses and noisy data. Either first or second derivatives help to give a general image of those features and structures.

Numerous methods were developed and frequently used among geophysicists to isolate and enhance gravity anomaly using its derivatives, such as horizontal gradient, analytic signal amplitude, and second vertical derivative.

Another anomaly enhancement method is the Generalized Derivative Operator (GDO) introduced by Cooper & Cowan (2011). It is a combination of first horizontal and vertical directional derivatives which are controlled by two angles, azimuth, and dip, and later divided by analytic signal amplitude. Cooper (2017; 2018), Cooper & Cowan (2011), and Khalil et al. (2015) show promising results of GDO to identify small and linear geological features.

Nevertheless, it is possible to perform derivation of potential field data on both spatial and frequency domains by mathematical approach. We use the finite difference (FD) for derivation in the spatial domain and fast Fourier transform (FFT) for derivation in the frequency domain. In this study, we adopt the Python package developed by Uieda et al. (2013) and Melo & Barbosa (2020) to perform the routine derivative and develop the GDO Python program.

Furthermore, this study is intended to recognize how to determine the appropriate angles of GDO and interpret the result of GDO which is later compared to analytic signal amplitude, horizontal gradient, and second vertical derivative. The other three derivative filters are used because all methods are widely applied to potential field data and are considered to be quite powerful to detect edges and anomalous bodies.

Various synthetic data and the Complete Bouguer Anomaly of Silver Peak are used to test GDO parameters. The CBA is filtered out from Alum and Silver Peak Complete Bouguer Anomaly data points using Verde (Uieda, 2018) module for acquiring only gravity data points around the Silver Peak area.

## 2. LITERATURE REVIEW

### *2.1. Silver Peak Geothermal Area*

Silver Peak area is part of the geothermal explorations in Esmeralda County, where the trans-tensional Walker Lane belt structure zone separates the Sierra Nevada block on the west and extensional Basin-Range on the east. According to the G&G report by Practical Geophysics (2008) and Hulen (2008) in **Figure 1**, there lays Goat Island horst-graben from Clayton Valley to Mineral Ridge. This feature acts as a hot fluid path for Silver Peak geothermal system.

Silver Peak geothermal system is a heat-sweep system, where a geothermal system is formed from hot deep fluid circulation in an active tectonic environment (continental

rifting (Hochstein & Browne, 2000) and does not associate with volcanism. Surface manifestation presence, Quaternary hot-spring sinter, points out the existence of this feature. The existence of horst-graben, high-angle fault, and granite in the Silver Peak geothermal area was identified from a previous gravity study (**Figure 1**). It is intriguing to inquire how GDO will enhance and isolate the anomaly of horst-graben, high-angle fault, and granite.

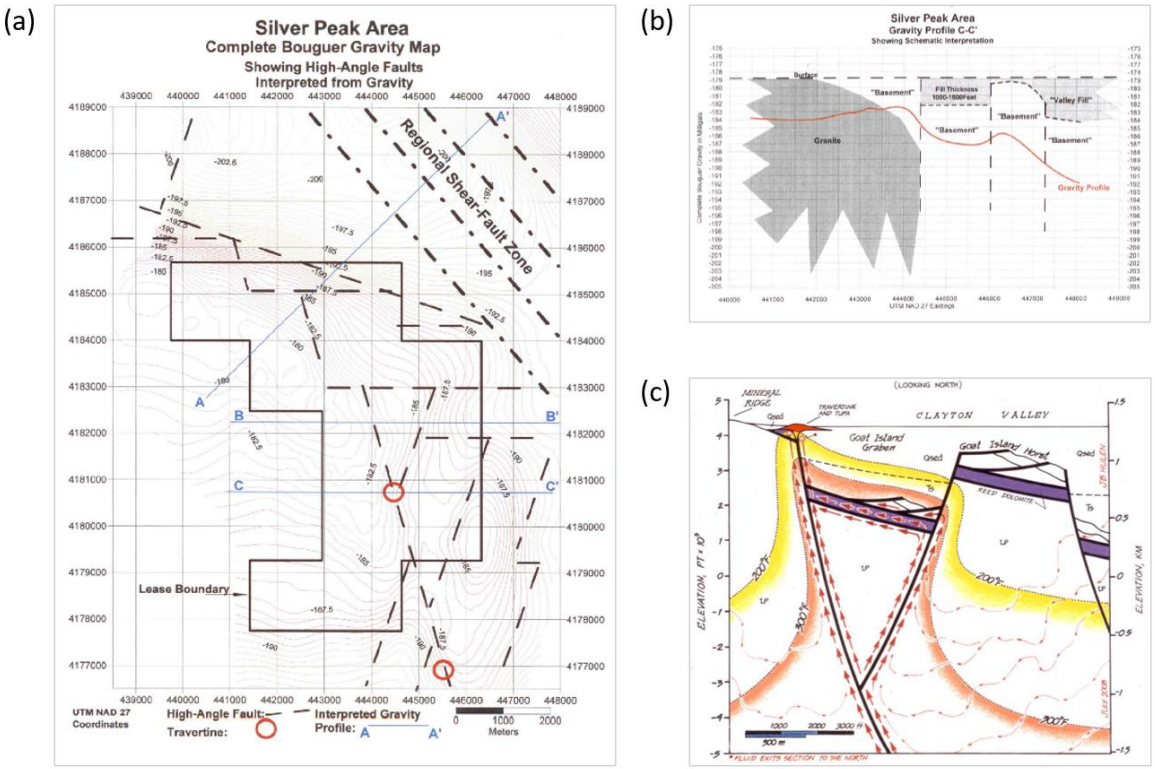


**Figure 1**. (a) Complete Bouguer Anomaly Map of Silver Peak Area with interpreted High-Angle Fault. (b) Cross Section of C-C' showing anomaly of gravity profile and schematic interpretation of High-Angle Fault (Practical Geophysics, 2008b). (c) Conceptual model of Silver Peak geothermal system which is controlled by complex fault system (Hulen, 2008).

### *2.2. Derivative of Gravity Data*

The derivative filters are based on the horizontal and vertical derivation of gravity data. The derivation is performed on the frequency and spatial domain using Fast Fourier Transform (FFT) and the central finite difference (FD) approach defined by Blakely (1995). For derivation on the frequency domain, the n-order derivatives of gridded gravity anomaly ($g_z$) on $x$, $y$, and $z$-axis were described by the equations as follows,

$$\frac{\partial^n g_z}{\partial x^n} = F^{-1}((ik_x)^n F(g_z)) \quad (1)$$

$$\frac{\partial^n g_z}{\partial y^n} = F^{-1}\left((ik_y)^n F(g_z)\right) \quad (2)$$

$$\frac{\partial^n g_z}{\partial z^n} = F^{-1}(|k_z|^n F(g_z)) \quad (3)$$

where,

$$|k_z|^n = \left(\sqrt{k_x^2 + k_y^2}\right)^n \quad (4)$$

$F$ is the FFT operator to transform spatial domain data ($g_z$) to the frequency domain and will be inverted back to the spatial domain using IFFT operator $F^{-1}$. The $n$ is the derivation order while $k$ is the wavenumber.

Padding and tapering were applied to the data before derivation using FFT to add extra columns and rows around the interpolated data matrix so that the grid dimensions would become even powers of two and also

add artificial values on the padded area to preserve the edges of the data matrix (Khalil et al., 2015).

Subsequently, the first derivative on the spatial domain was performed using finite-difference which is described by the equation as follows,

$$\frac{\partial g_z}{\partial x} = \frac{g_{z_{i+1,j}} - g_{z_{i-1,j}}}{2\Delta x} \quad (5)$$

$$\frac{\partial g_z}{\partial y} = \frac{g_{z_{i,j+1}} - g_{z_{i,j-1}}}{2\Delta y} \quad (6)$$

$i$ and $j$ are indices of 2D matrix $g_z$ which correspond with $x$ and $y$-direction. $\Delta x$ and $\Delta y$ are the distance of grid points.

## 3. DATA AND METHODS

### *3.1. Derivative Operator*

The derivative operator is developed based on variation and association between derivatives of the potential field in the $x$, $y$, and $z$ axes which is already described in Section 2.2.

The derivative operator such as horizontal gradient, analytic signal amplitude, and second vertical derivative will result in a higher frequency response that enhances and localizes the response of the source.

In this paper, the results from GDO and common derivative operator, are compared by applying them to the synthetic data and field data. **Table 1** shows the equation of Generalized Derivative Operator (GDO) and derivative operator that is used in this paper.

**Table 1**. Derivative operator equation.

| Derivative Operator | Formula |
|---|---|
| Horizontal gradient (HG) | $H = \sqrt{\left(\frac{\partial f}{\partial x}\right)^2 + \left(\frac{\partial f}{\partial y}\right)^2}$ (7) |
| Analytic Signal Amplitude (AS) | $AS = \sqrt{\left(\frac{\partial f}{\partial x}\right)^2 + \left(\frac{\partial f}{\partial y}\right)^2 + \left(\frac{\partial f}{\partial z}\right)^2}$ (8) |
| Second Vertical Derivative (SVD) | $\frac{\partial^2 g_z}{\partial z^2} = -\frac{\partial^2 g_z}{\partial x^2} - \frac{\partial^2 g_z}{\partial y^2}$ (9) |
| Generalized Derivative Operator (GDO) | $GDO = \frac{\frac{\partial f}{\partial \theta \partial \phi}}{AS} = \frac{\left(\frac{\partial f}{\partial x}\sin\theta + \frac{\partial f}{\partial y}\cos\theta\right)\cos\phi + \frac{\partial f}{\partial z}\sin\phi}{\sqrt{\left(\frac{\partial f}{\partial x}\right)^2 + \left(\frac{\partial f}{\partial y}\right)^2 + \left(\frac{\partial f}{\partial z}\right)^2}}$ (10) |

### *3.2. Generalized Derivative Operator*

The Generalized Derivative Operator (GDO) is defined as a directional derivative filter. Mlsna and Rodríguez (2009) defines "2D directional derivative" by,

$$\frac{\partial f}{\partial \theta} = \frac{\partial f}{\partial x}\cos\theta + \frac{\partial f}{\partial y}\sin\theta \quad (11)$$

with $\theta$ as an angle to the horizontal $x$-axis, assuming the axis has an east-west orientation. Its angle is reversed by Cooper & Cowan (2011) to follow the azimuth of the geographic coordinates, changing equation (11) to be,

$$\frac{\partial f}{\partial \theta} = \frac{\partial f}{\partial x}\sin\theta + \frac{\partial f}{\partial y}\cos\theta \quad (12)$$

To derive the function on a 3D vector, "3D directional derivative" can be defined as equation (13) by following equation (12) to derive the function between the horizontal plane and vertical $z$-axis.

$$\frac{\partial f}{\partial \theta \partial \phi} = \left(\frac{\partial f}{\partial x}\sin\theta + \frac{\partial f}{\partial y}\cos\theta\right)\cos\phi$$

$$+\frac{\partial f}{\partial z}\sin\phi \quad (13)$$

$$\frac{\partial f}{\partial \theta \partial \phi} = \left(\frac{\partial f}{\partial x}\sin\theta + \frac{\partial f}{\partial y}\cos\theta\right)\cos\phi + \frac{\partial f}{\partial z}\sin\phi \quad (14)$$

$\phi$ is an angle between the horizontal plane and the vertical $z$-axis. If equation (13) is normalized by analytic signal, equation (8), then the formula of GDO is obtained, equation (10). Following Cooper (2018), choosing $\theta$ follows the orthogonal of the structure strike.

The direction of various derivative operators in 3D space is illustrated in **Figure 2**. Note that the potential field $f$ for gravity data is Bouguer anomaly, the gravity field in the $z$-direction. GDO which is based on a "3D directional derivative" will give the flexibility to control the direction of the derivative. Subsequently, the enhanced anomaly will be maximized and correspond with the desired orientation of the anomalous body.

GDO is also normalized with AS, which will return values between -1 to 1. As seen in **Figure 2**, if the "3D directional derivative" is aligned and has the same direction with AS, the GDO value will be 1. Conversely, if the "3D directional derivative" has the opposite direction with AS, the GDO value will be -1. The opposite direction means a negative value obtained from the derivative of the potential field in the horizontal direction of $x$ and $y$.

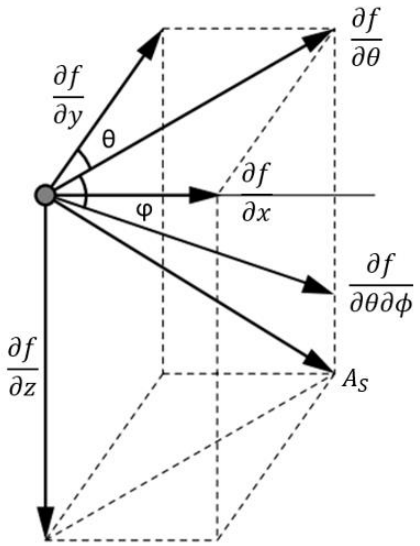


**Figure 2**. The direction of various derivative operators in 3D space (Cooper & Cowan, 2011).

### *3.3. Synthetic Data*

This study uses Bouguer anomaly synthetic data which is obtained from forward modeling of simple prisms. We utilize Harmonica by Soler et al. (2021) which is a Python package that provides forward modeling function of a simple geometry shape. The boundary and density contrast of the prism model are varied to obtain different responses. **Figure 3** shows the map of gravity anomaly response from 3 models and **Table 2** shows the detail parameter of the synthetic model.

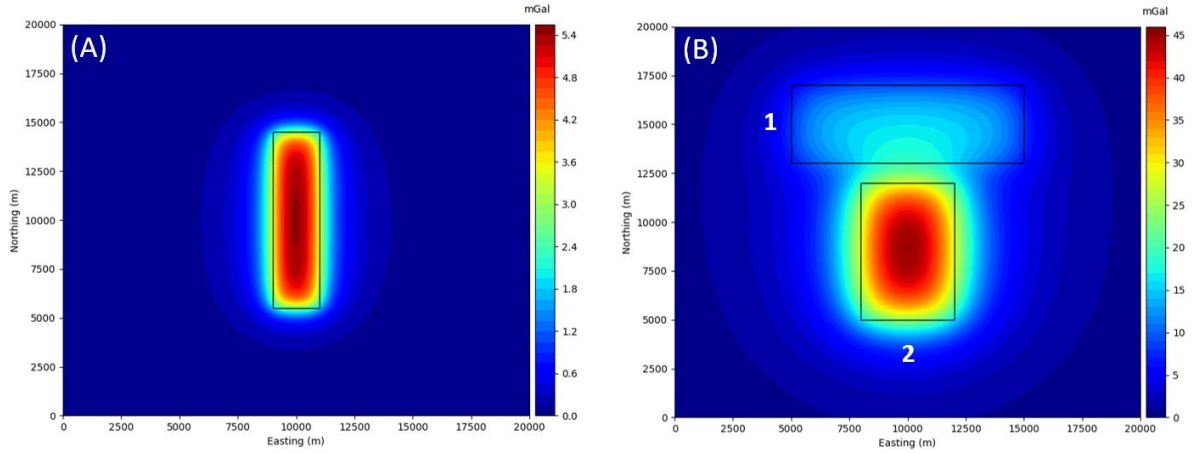


**Figure 3**. Bouguer anomaly map of synthetic data of 3 model, the label model corresponds with detail parameter in Table 2. Solid lines denote the edges of the model prisms.

**Table 2**. Parameter of the synthetic model.

| Parameter | Model A | Model B |
|---|---|---|
| Density Contrast | 1000 kg/m$^3$ | Prism 1: 1000 kg/m$^3$<br>Prism 2: 2000 kg/m$^3$ |
| Upper boundaries | -500 m | Prism 1: -1000 m<br>Prism 2: -1000 m |
| Lower boundaries | -700 m | Prism 1: -1500 m<br>Prism 2: -2000 m |
| Grid Size | 100 m x 100 m | |
| Area size | 20 km x 20 km | |

Model A is only 1 simple prism with a density contrast of 1000 kg/m$^3$ which is buried at a depth of 500 m (Upper Boundary). This model is set such that has an N-S strike. Model A is expected to denote local response.

Conversely, Model B consists of 2 prisms that are varied in strike orientation. Prism 1 with E-W strike and 1000 kg/m$^3$ density contrast, as well as prism 2 with N-S strike and 2000 kg/m$^3$ density contrast. Furthermore, the prisms have a deeper depth at 1000 m. Model B represents the regional anomaly response.

### *3.4. Silver Peak Gravity Data*

In this paper, we use gravity field data of Silver Peak which is generated from the Silver Peak Innovative Exploration Project (Ram Power Inc, 2013). The data is publicly accessible in Geothermal Data Repository (http://gdr.openei.org/submissions/268).

The Complete Bouguer Anomaly (CBA) data of Silver Peak is covering a 12 km x 14 km area with grid spacings of 0.25 km to 1.6 km (0.5 mi). The Bouguer density is 2.35 g/cc with NAD83 datum (Magee, 2009). The CBA map described in **Figure 4a** is interpolated data field by using the Kriging method with 100 m x 100 m grid sizes. Additionally, the geological map of Silver Peak is shown in **Figure 4b**.

The Silver Peak area lithologies consist of Cambrian dolomitized-marble (Cr), Proterozoic Wyman formation (pCw), Cambrian Deep Spring formation (Cds), Cambrian Poleta formation (Cp), Mesozoic granitoid intrusive rocks (Tlg), Quaternary playa deposits (Qp), Quaternary/Tertiary basalt (Qlb) and Quaternary alluvial deposits (Qaf). Quaternary hot-spring sinter is present which consists of travertine and tuff (Qs). Lithologies older than Quaternary deposits are known as Mineral Ridge in the Silver Peak, which deforms by cross-central faults.

It can be understood that the CBA anomaly is highly related to the response of the lithological contact, as seen by comparing between CBA map and geological map. The pattern of relatively high CBA anomaly (red - yellowish) is similar to the existence of Cr, pCw, and Tlg lithology. The medium CBA anomaly (greenish) also occurs with the existence of alluvial deposits (Qaf).

Conversely, the existence of structures such as graben, high-angle fault, and granite is hardly detected on the CBA map. Subsequently, anomaly enhancement with derivative operator might be interesting to be carried out.

## 4. RESULTS AND DISCUSSION

### *4.1. GDO of Synthetic Data*

Essentially, the test on synthetic data will provide an understanding of GDO behavior as performed by Cooper & Cowan (2011) and Cooper (2018). Consequently, we attempt the GDO on synthetic Bouguer anomaly from the prism model described in **Table 2**, which is generated using the Harmonica Python package by Soler et al. (2021). In this attempt, we compare GDO with its underlying formula, which is 2D and 3D directional derivatives.

**Figure 5** describes the 2D directional derivative, 3D directional derivative, and GDO anomaly map of the synthetic Model A.

The 2D directional derivative with $\theta = 45^o$ results in both high (red) and low (blue) anomalies which are concurred with the edges of the prism model (**Figure 5a**). Furthermore, the 3D directional derivative will amplify the response of the geometry body from the prism model (**Figure 7b**), which is quite similar to the response of AS. High anomalies appear to be the geometry of its source with low anomalies surrounding the source.

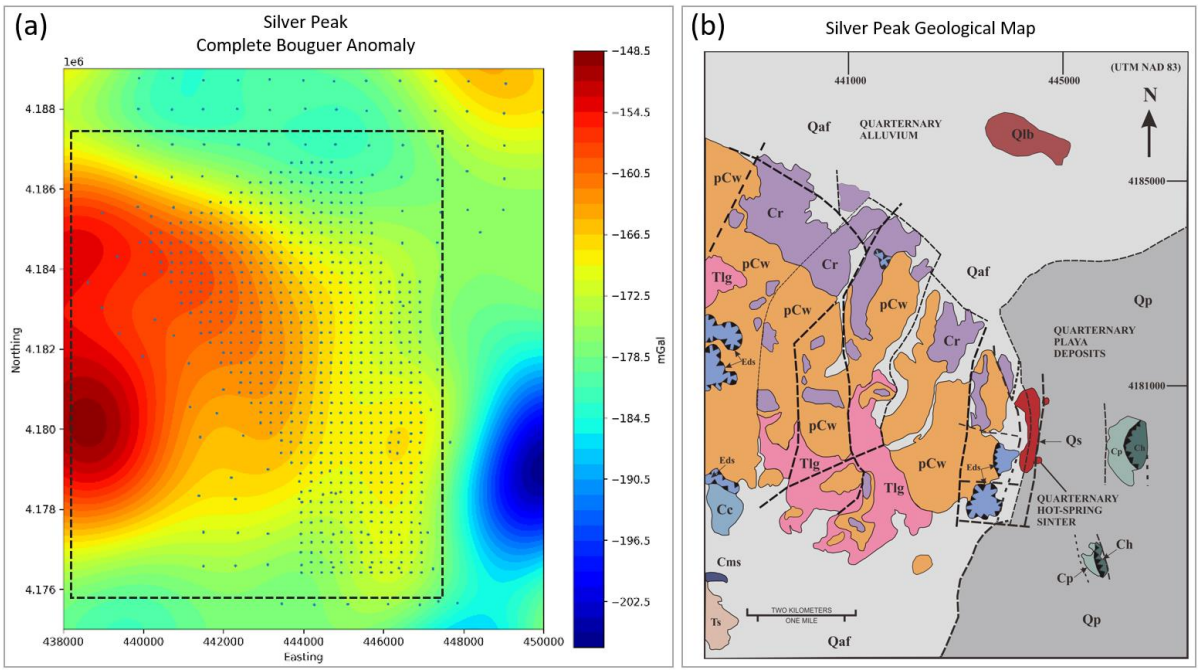


**Figure 4**. (a) Complete Bouguer Anomaly map of Silver Peak area. (b) The geological map of Silver Peak area, modified from Hulen (2008) and Western Geothermal Partners LLC (2006). Note that the dashed-line rectangular on the CBA map denotes the covered area of the geological map.

Moreover, GDO is the ratio of 3D directional derivative and AS. If we use $\theta = 90^o$ and $\phi = 0^o$, the east edge of the source shows high anomalies (red) and the west edge of the source shows low anomalies (blue) as shown in **Figure 5c**. On the other hand, **Figure 5d** shows if we use $\theta = 0^o$ and $\phi = 0^o$, the north edge of the source shows low anomalies (blue) and the south edge of the source shows high anomalies (red). From these trials, we can understand that $\phi = 0^o$ only leaves the horizontal derivatives ($x$ and $x$) that follows the direction of the azimuth ($\theta$).

**Figure 5e** shows the GDO response where $\theta = 0^o$ and $\phi = 90^o$. According to equation (10) of GDO, the use of $\phi = 90^o$ only leaves the vertical derivative and won't respond to any horizontal derivatives with different azimuths. Last, **Figure 5f** shows the GDO response where $\theta = 30^o$ and $\phi = 60^o$. We can see that the response of GDO follows the direction of the azimuth ($\theta$). Yet the enhanced anomaly slightly misses the actual location of the prism.

As suggested by Cooper (2018) the value of azimuth ($\theta$) of the GDO parameters should follow the orthogonal direction of the structure strike. In this research, we have a limitation on the prism model which only could have N-S or W-E strike orientation. Consequently, the attempt on GDO using $\theta = 30^o$ (**Figure 5f**) will be more suitable if the prism model used has a strike with azimuth $120^o$.

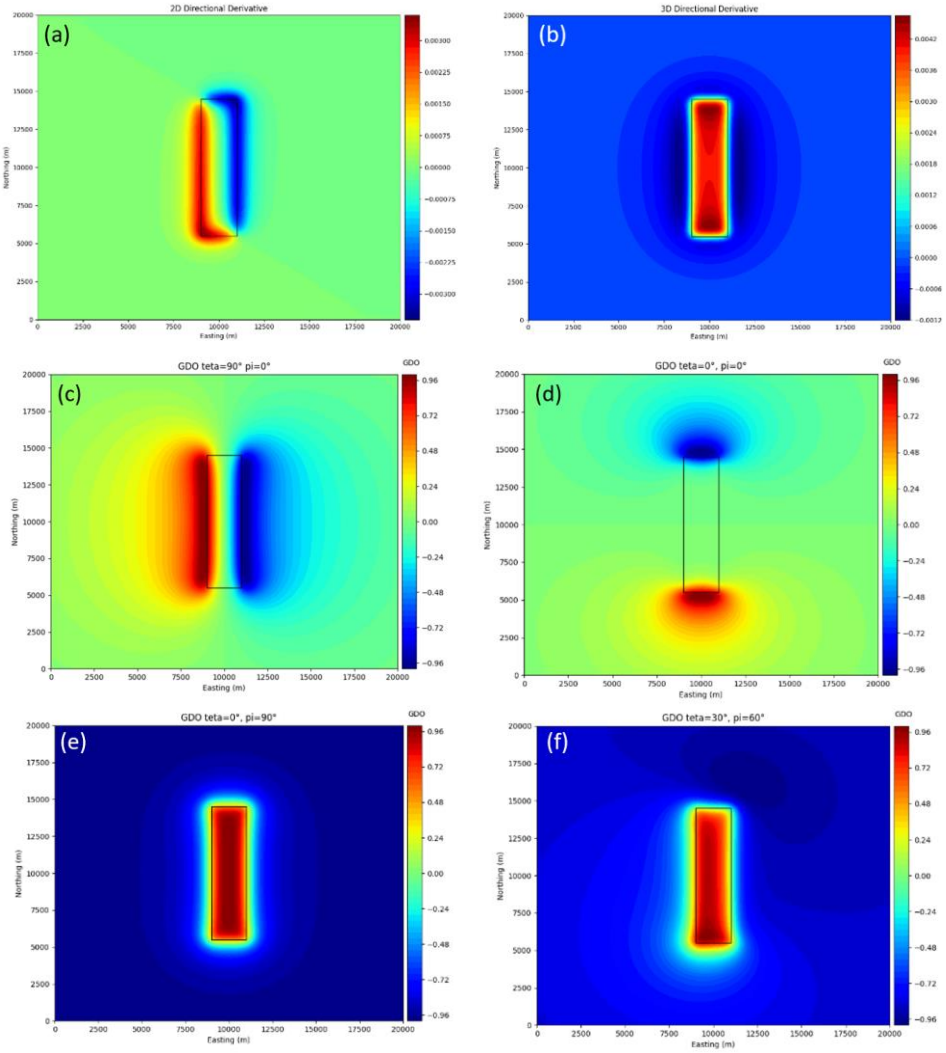


**Figure 5**. (a) 2D directional derivative with $\theta = 45^o$; (b) 3D directional derivative with $\theta = 45^o$, $\phi = 90^o$; (c) GDO with $\theta = 90^o$, $\phi = 0^o$; (d) GDO $\theta = 90^o$, $\phi = 90^o$; (e) GDO $\theta = 0^o$, $\phi = 90^o$; (f) GDO $\theta = 30^o$, $\phi = 60^o$.

### *4.2. Comparing GDO with SA, HG, and SVD*

We compare the result from GDO with common derivative operators such as SA, HG, and SVD. **Figure 6** shows the results of GDO, SA, HG, and SVD based on synthetic Bouguer anomaly from Model A. As seen in **Figure 6**, all derivative operators have successfully enhanced the response anomaly of the shallow depth prism (Model A). It is denoted by the anomaly pattern that concurs with the edges of the prism. Anomaly profiles from all derivative operators are also exhibited to obtain detailed perspectives between edges response and the anomaly pattern.

The GDO anomaly of $\theta$ = 0$^o$ and $\phi$ = 90$^o$ shows maximum values concurring with the prism geometry (**Figure 8a**). It is observed from the GDO profile that a significant decreasing value occurred near the edges of the prism (red-dashed line).

Nevertheless, analytic signal amplitude returns a ridge-like response where high values are near the edges of the prism and slightly decreases at the center of the prism (**Figure 6b**). Meanwhile, the horizontal gradient shows maximum values at the edges of the prism and zero values at the center of the prism (**Figure 6c**). HG and 2D directional derivatives with $\theta$ = 45$^o$ are derivative operators in the horizontal plane which return similar patterns (**Figure 5a** and **Figure 6c**), though the 2D directional derivative has positive and negative values that concur with the edges of the prism.

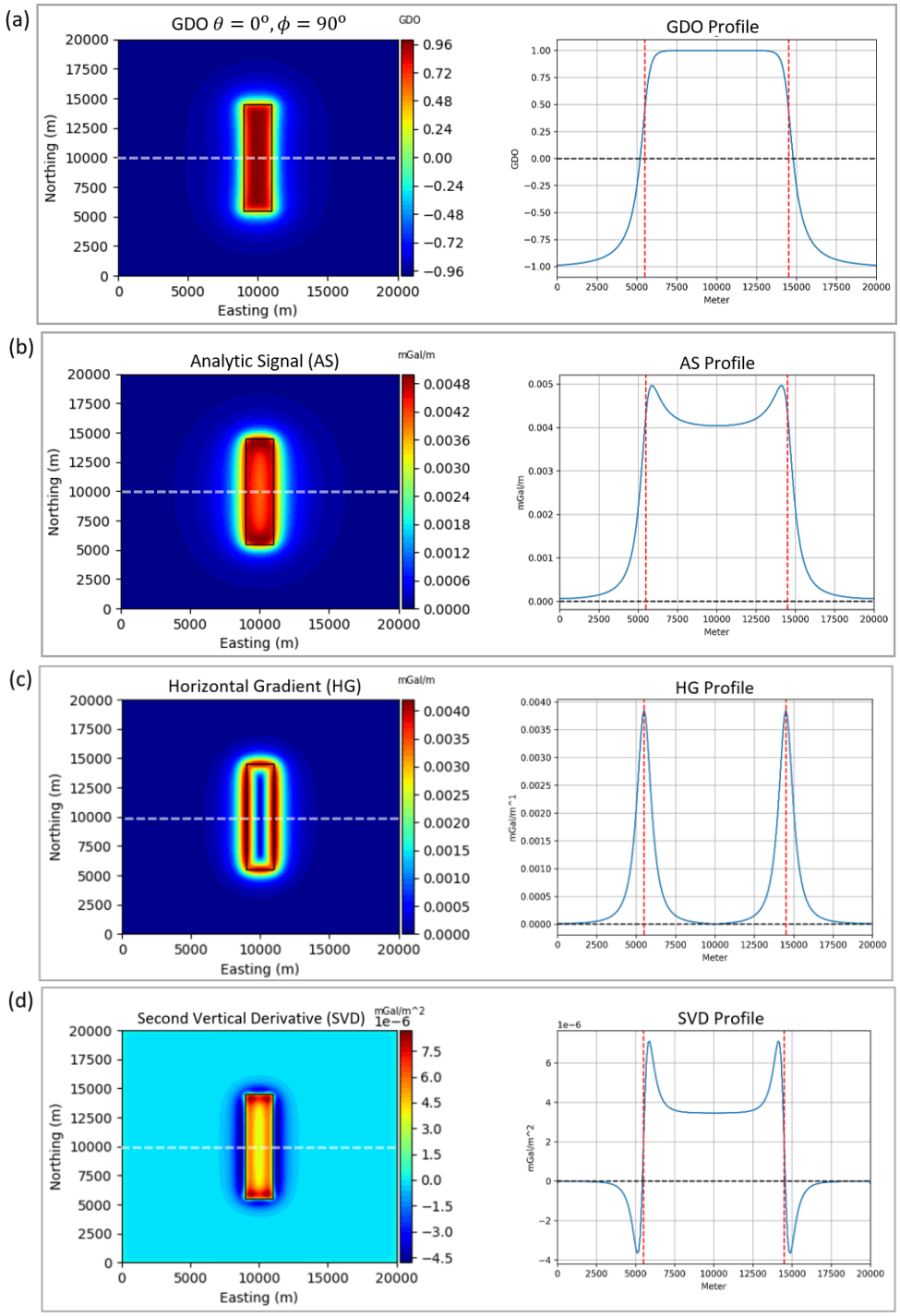


**Figure 6**. Results comparison of (a) GDO $\theta = 0^o$ and $\phi = 90^o$, (b) Analytic Signal Amplitude (AS), (C) Horizontal Gradient (HG), (D) Second Vertical Derivative (SVD) based on the local anomaly of synthetic model A. On the profile, red-dashed lines denote the edges of the prism and the black-dashed line is zero value level.

Besides, the Second Vertical Derivative (SVD) anomaly is estimated from the second derivative in the $x$ and $y$ directions (Equation 9). The SVD operator will return the curvature of the Bouguer anomaly, which means the changes in the dip direction of the anomaly. As seen in Figure 6d, the edge of the prism (red-dashed line) concurs with zero value between the maximum and minimum value of SVD (Sumintadireja et al., 2018).

Equally important, the comparison between derivative operators is carried out for regional anomaly. We use synthetic Bouguer anomaly from Model B (**Figure 3b**) consisting 2 prisms with deeper depth.

As observed in **Figure 3b**, the Bouguer anomaly response of prism 1 is lower than prism 2 due to smaller density contrast. The Bouguer map indicates two sources of anomaly although the geometry of the sources is hardly identified.

**Figure 7** shows the result of different derivative filters on synthetic regional anomaly from Model B. Unequal with the derivative result of local anomaly from Model A, which is concurred with the prism geometry, the anomaly of the deeper source from Model B fails to be amplified with operator AS, HG, and SVD, especially for the response of prism 1.

It appears that the anomaly response of prism 2 with higher contrast density is enhanced by AS, HG, and SVD. Nevertheless, the pattern of enhanced anomaly is not matched on the edges of the prism. Yet SVD anomaly is able to elucidate the boundary.

Conversely, GDO can amplify the response of the deeper source body, which is described by a high anomaly with the value of 0.7 higher (red color). If we compare the result of GDO between the local anomaly of model A and the regional anomaly of model B, it appears that enhanced anomalies are slightly not matched with the geometry of the prisms. Nonetheless, the response from prism 1 is successfully enhanced by GDO.

From several tests of synthetic data, we conclude that GDO tends to amplify the anomaly, regardless of the value of the Bouguer anomaly, as well as the medium value which could be caused by lower density contrast or deeper location of the anomalous source. Thus, we should be cautious when interpreting the GDO anomaly and should compare the result with the Bouguer anomaly and geological map.

### *4.3. GDO of Silver Peak Area*

Various derivative operators are applied to the Complete Bouguer Anomaly from the Silver Peak area. We try GDO by varying the azimuth ($\theta$) & dip ($\phi$), and another derivative operator of AS, HG, and SVD as well, the results are described in **Figure 8**.

We reconcile on the geological map (**Figure 4b**) to interpret the enhanced anomaly from the derivative operators. The structure of horst-graben plays an important role as the geothermal fluid pathway on Silver Peak geothermal system as well as the intrusive granite in the Mineral Ridge area. To interpret the GDO anomaly, we try to follow the suggestion of Cooper (2018) where $\pm 1/\sqrt{2}$ GDO might be contacts and zero GDO appears to be dykes.

It appears that AS and HG fail to enhance the anomaly at the Silver Peak area (**Figures 8a** and **8b**). The expected response from horst-graben and intrusive granite is not revealed from AS and HG results.

Conversely, SVD and GDO can amplify the response of possible horst-graben and intrusive granite (**Figure 8c** and **8d**). It appears that the potential field responses of those geological structures are more sensitive to the changes in the vertical direction (vertical derivative). Consequently, we deduce that this might be related to the geometry of high-angle faults including horst-graben structures in the Silver Peak area (Hulen, 2008).

Furthermore, by referring to the geological map, there lays a cross-central fault system that separates Clayton Valley and Mineral Ridge. This fault might extend to the south across the horst-graben from GDO and SVD results.

Comparing the GDO results of **Figures 8d**, **8e**, and **8f**, it appears that varying the dip parameter ($\phi$) of the GDO will enhance the anomaly in certain ways. For instance, in **Figure 8f** we use $\phi = 30^{o}$ and the horst anomaly appears as narrow closure. Nevertheless, in **Figure 8d** and **8e**, the horst anomaly become more extensive.

Subsequently, opposite behavior is observed for intrusive granite structures in the Mineral Ridge area. Granite anomaly appears extensively in lower dip GDO (**Figure 8f**) rather than in higher dip GDO (**Figures 8d** and **8e**). Meanwhile, the response from lithology of basalt strongly appears in GDO $\theta = 45^{o}$ and $\phi = 75^{o}$

(**Figure 8e**) rather than in others (**Figure 8d** and **8f**).

Consequently, we could conclude that GDO is able to enhance the anomaly of the potential field with several possibilities by varying its parameters of azimuth ($\theta$) and dip ($\phi$). Tuning the GDO parameters in certain ways might reveal the edge response of complex geological structures which might not appear in ordinary derivative operators. Examining the correlation between $\theta$ and $\phi$ of GDO with the various orientation and dip of know source anomaly might be intriguing to be validated in future work.

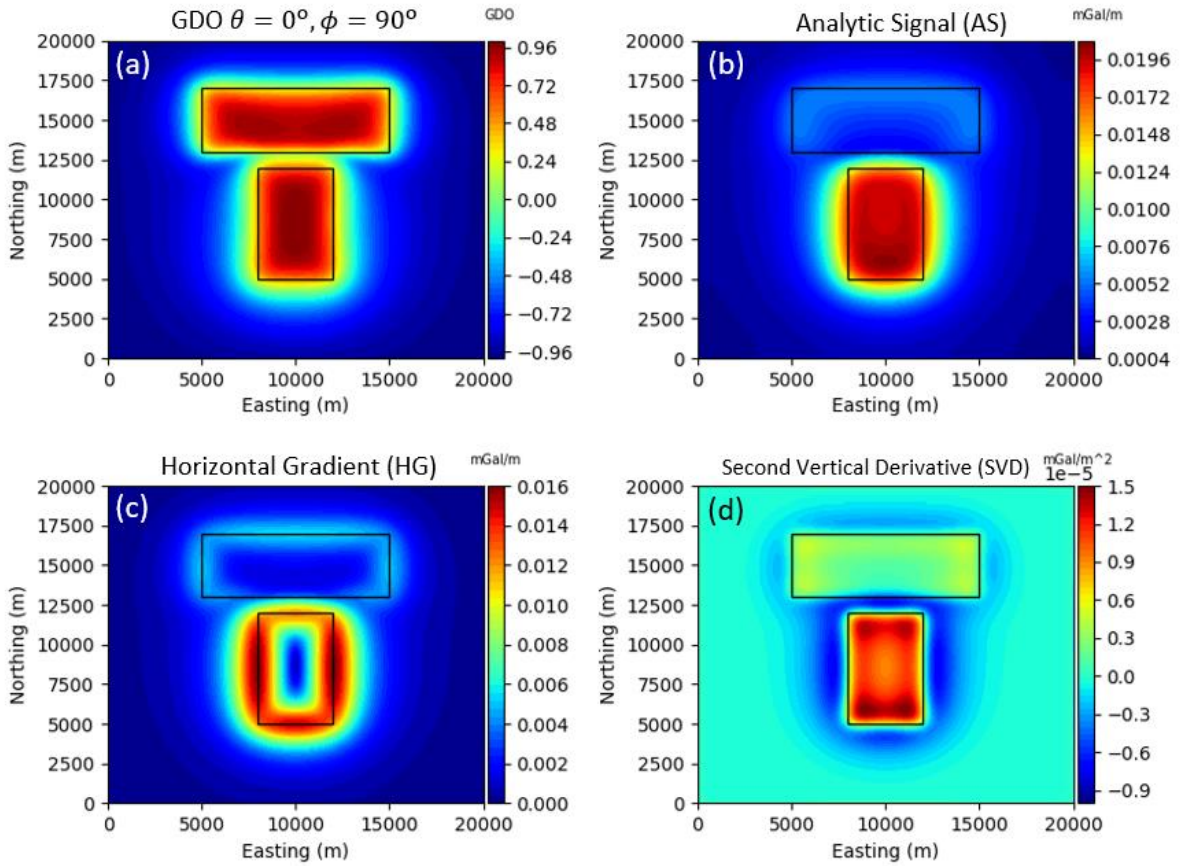


**Figure 7**. Results comparison of (a) GDO $\theta = 0^o$ and $\phi = 90^o$, (b) Analytic Signal Amplitude (AS), (C) Horizontal Gradient (HG), (D) Second Vertical Derivative (SVD) based on the regional anomaly of synthetic model B.

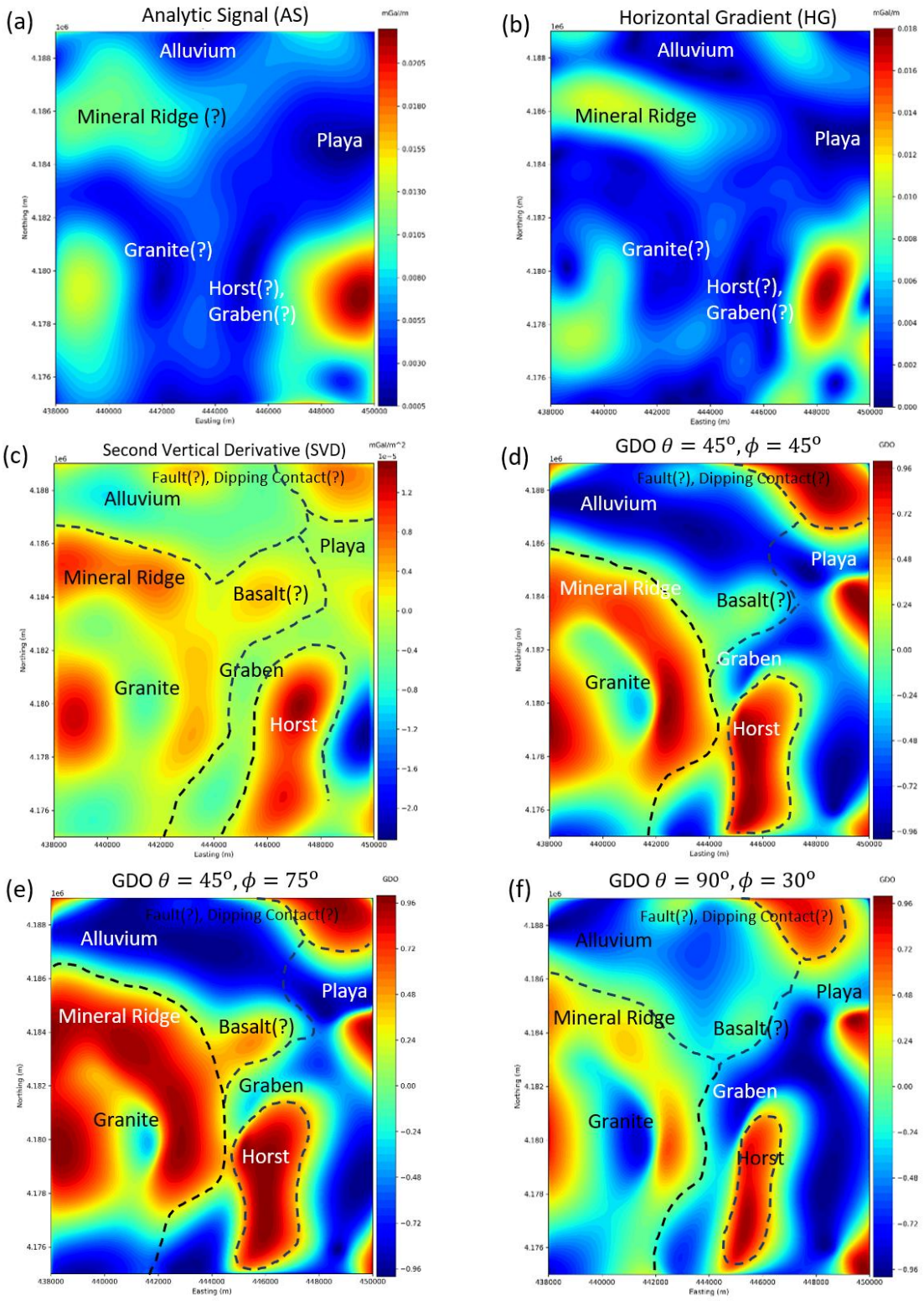


**Figure 8**. Interpreted of enhanced anomaly from (a) Analytic Signal Amplitude (AS), (b) Horizontal Gradient (HG), (c) Second Vertical Derivative (SVD), (d) GDO $\theta = 45^o$ and $\phi = 45^o$, (e) GDO $\theta = 45^o$ and $\phi = 75^o$, (f) GDO $\theta = 90^o$ and $\phi = 30^o$.

## 5. CONCLUSION

In this study, we examine GDO parameters and compare them with other derivative operators, both on synthetic and field Bouguer anomalies. Thus, we conclude that,

a. The results from synthetic data show that GDO can amplify the response both on local and regional anomalies. Apparently, the enhancement anomaly of GDO disregards the influence of density contrast and depth of the anomalous body. This is a consequence of the normalization factor where GDO is basically, a 3D directional derivative that normalizes with Analytic Signal Amplitude (Equation 10). Thus, we should be cautious when interpreting the GDO anomaly and should compare the result with the Bouguer anomaly and geological map.
b. The anomaly enhancement of the Silver Peak area elucidates the GDO anomaly concurred with the geological map. The response from the horst-graben structures and intrusive granite is managed to be amplified by GDO. The SVD can amplify the response of horst-graben as well, though AS and HG do not show the same results.
c. GDO can enhance the anomaly of the potential field, revealing the edges response of complex geological structures that might not appear in ordinary derivative operators.

## ACKNOWLEDGMENT

The authors thank Anonymous Reviewers for their advice on this manuscript. We credit Ram Power, Inc. for providing the Silver Peak field data publicly. We thank the Geophysical Engineering Department and Center for Geosciences Artificial Intelligence and Advanced Computing, Universitas Pertamina for supporting this research.

## REFERENCE

Blakely, R. J. (1995). *Potential Theory in Gravity and Magnetic Applications*. Cambridge University Press. https://doi.org/10.1017/CBO9780511549816

Cooper, G. R. J. (2017, September 12). Generalising the GDO. *15th South African Geophysical Association Biennial Conference & Exhibition.* .

Cooper, G. R. J. (2018). The Interpretation of The Generalised Derivative Operator. *Geophysical Prospecting*, *66*(1), 197–206. https://doi.org/10.1111/1365-2478.12539

Cooper, G. R. J., & Cowan, D. R. (2011). A Generalized Derivative Operator for Potential Field Data‡. *Geophysical Prospecting*, *59*(1), 188–194. https://doi.org/10.1111/j.1365-2478.2010.00901.x

Hochstein, M. P., & Browne, P. R. L. (2000). *Surface Manifestations of Geothermal System with Volcanic Heat Sources*. In H. Sigurdsson, B. Houghton, S. McNutt, H. Rymer, & J. Stix (Eds.), The Encyclopedia of Volcanoes (1st ed., pp. 835–855). Academic Press.

Hulen, J. B. (2008). *Geology and Conceptual Modelling of the Silver Peak Geothermal Prospect, Esmeralda County, Nevada*. https://doi.org/10.15121/1148794

Khalil, M. A., Santos, F. M., Farzamian, M., & El-Kenawy, A. (2015). 2-D Fourier Transform Analysis of The Gravitational Field of Northern Sinai Peninsula. *Journal of Applied Geophysics*, *115*, 1–10. https://doi.org/10.1016/j.jappgeo.2015.01.022

Magee, C. (2009). *Gravity Survey over the Silver Peak Prospect, Esmeralda County, Nevada*.

Melo, F. F., & Barbosa, V. C. F. (2020). Reliable Euler Deconvolution Estimates Throughout The Vertical Derivatives of The Total-Field Anomaly. *Computers & Geosciences*, *138*, 104436. https://doi.org/10.1016/j.cageo.2020.104436

Mlsna, P. A., & Rodríguez, J. J. (2009). Gradient and Laplacian Edge Detection. In *The Essential Guide to Image Processing* (pp. 495–524). Elsevier. https://doi.org/10.1016/B978-0-12-374457-9.00019-6

Practical Geophysics (2008). *Silver Peak/Alum Geothermal Areas, Esmeralda County, Nevada: Interpretation of Gravity Survey*. https://doi.org/10.15121/1148793

Ram Power Inc. (2013). *Silver Peak Innovative Exploration Project (Ram Power Inc) [set data]*.

Soler, S. R., Uieda, L., Oliveira Jr, V. C., Shea, N., & Pesce, A. (2021). Forward Modeling, Inversion, and Processing Gravity and Magnetic Data. In *Harmonica*.

Sumintadireja, P., Dahrin, D., & Grandis, H. (2018). A Note on the Use of the Second Vertical Derivative (SVD) of Gravity Data with Reference to Indonesian Cases. *Journal of Engineering and Technological Sciences*, *50*(1), 127–139. https://doi.org/10.5614/j.eng.technol.sci.2018.50.1.9

Uieda, L. (2018). Verde: Processing and gridding spatial data using Green's functions. *Journal of Open Source Software*, *3*(30), 957. https://doi.org/10.21105/joss.00957

Uieda, L., Oliveira, V., & Barbosa, V. (2013). *Modeling the Earth with Fatiando a Terra*. 92–98. https://doi.org/10.25080/Majora-8b375195-010

Western Geothermal Partners LLC. (2006). *Silver Peak Geothermal Prospect, Esmeralda County, Nevada-Direct Use Potential*. https://doi.org/10.15121/1148794